ACS ES&T Air

pubs.acs.org/estair

Article

Divergent Adhesion–Proliferation Profiles in 16HBE Cells May Contribute to Differential Risk Assessment of *P. aeruginosa* Bioaerosol Exposure: Primary NHBE Comparison

Yunyun Zhang, Guiying Li,* Zhishu Liang, Po Keung Wong, and Taicheng An

Cite This: https://doi.org/10.1021/acsestair.5c00326

Read Online

ACCESS | Metrics & More | Article Recommendations | Supporting Information

ABSTRACT: Bioaerosols are important components of atmospheric aerosols. Substantial evidence demonstrates a significant positive association between bioaerosol exposure and adverse respiratory outcomes, yet accurate health risk assessment remains constrained due to inadequate *in vitro* exposure models. Thus, an exposure system at the air–liquid interface was established to simulate exposure of environmentally relevant *Pseudomonas aeruginosa*(*P. aeruginosa* bioaerosol to respiratory epithelial cells. The primary normal human bronchial epithelial (NHBE) cells and immortalized 16HBE cell line were used as comparative exposure models. NHBE cells exhibited significantly higher sensitivity to 10^5 CFU/m^3 *P. aeruginosa* bioaerosol, with cell viability decreasing by 58.3% ± 1.4% in NHBE cells versus 43.8% ± 14.9% in 16HBE cells ($p < 0.05$). Distinct immune recognition mechanisms were further observed, and 16HBE cells recognized *P. aeruginosa* through toll-like receptors, RIG-I-like receptors (RLRs), NOD-like receptors (NLRs), and cytosolic DNA-sensing (cGAS-STING), whereas NHBE cells primarily relied on NLRs, triggering a distinct downstream immune effector. Further, immortalization of cells resulted in baseline alterations. 16HBE cells demonstrated impaired barrier integrity and reduced proliferative capacity but compensatory hyperactivation of pattern recognition receptors, whereas NHBE cells mounted a comprehensive immune response concurrent with greater cytotoxicity. Reduced cytotoxicity of the *P. aeruginosa* bioaerosol in 16HBE cells underestimated bioaerosol risk significantly. This study elucidated functional disparities between immortalized cells and primary cells and revealed the limitation of cell lines in health risk assessment.

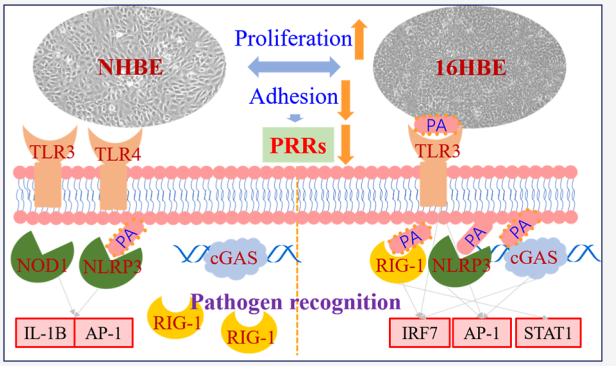

KEYWORDS: *Pseudomonas aeruginosa bioaerosol, cytotoxicity, exposure model, pattern recognition receptor, immune response*

1. INTRODUCTION

The global coronavirus disease 2019 (COVID-19) pandemic underscores the critical role of bioaerosols in airborne disease transmission.[1,2] Aerosolized pathogens can remain viable in the atmosphere for prolonged periods,[3] posing considerable risks of respiratory infections,[4] particularly among immunocompromised individuals.[5−7] Epidemiological evidence establishes a strong correlation between bioaerosol exposure and various adverse respiratory outcomes.[8,9] However, the environmental health risks posed by bioaerosols remain incompletely understood owing to their complex composition, dynamic physicochemical properties, and unique biological behavior.

Accurate *in vitro* exposure systems are essential for quantifying bioaerosol health risks. The accuracy of these systems is significantly influenced by several factors, including bioaerosol physicochemical properties, exposure approaches, and particularly the inoculation method.[10] *Pseudomonas aeruginosa* (*P. aeruginosa*), an opportunistic pathogen frequently found in bioaerosols,[11,12] accounts for approximately 16% of clinical infections and 23% of ICU-acquired infections,[13] making it a suitable model microorganism of bioaerosols. Submerged exposure approaches are widely used for potential health risk assessment of numerous pollutants, including organics and nanoparticles,[14,15] but they fail to replicate aerosol deposition dynamics and may alter aerosol physicochemical properties.[16] Comparatively, air–liquid interface (ALI) exposure approaches more accurately mimic the *in vivo* respiratory environment.[17] Although direct bacterial suspension inoculation offers a cost-effective and rapid method,[18] aerosolization significantly alters the viability and morphology of pathogens, thereby affecting their infectivity in the aerosolized form.[19] Thus, this study established an ALI

Received: August 25, 2025
Revised: December 29, 2025
Accepted: December 29, 2025

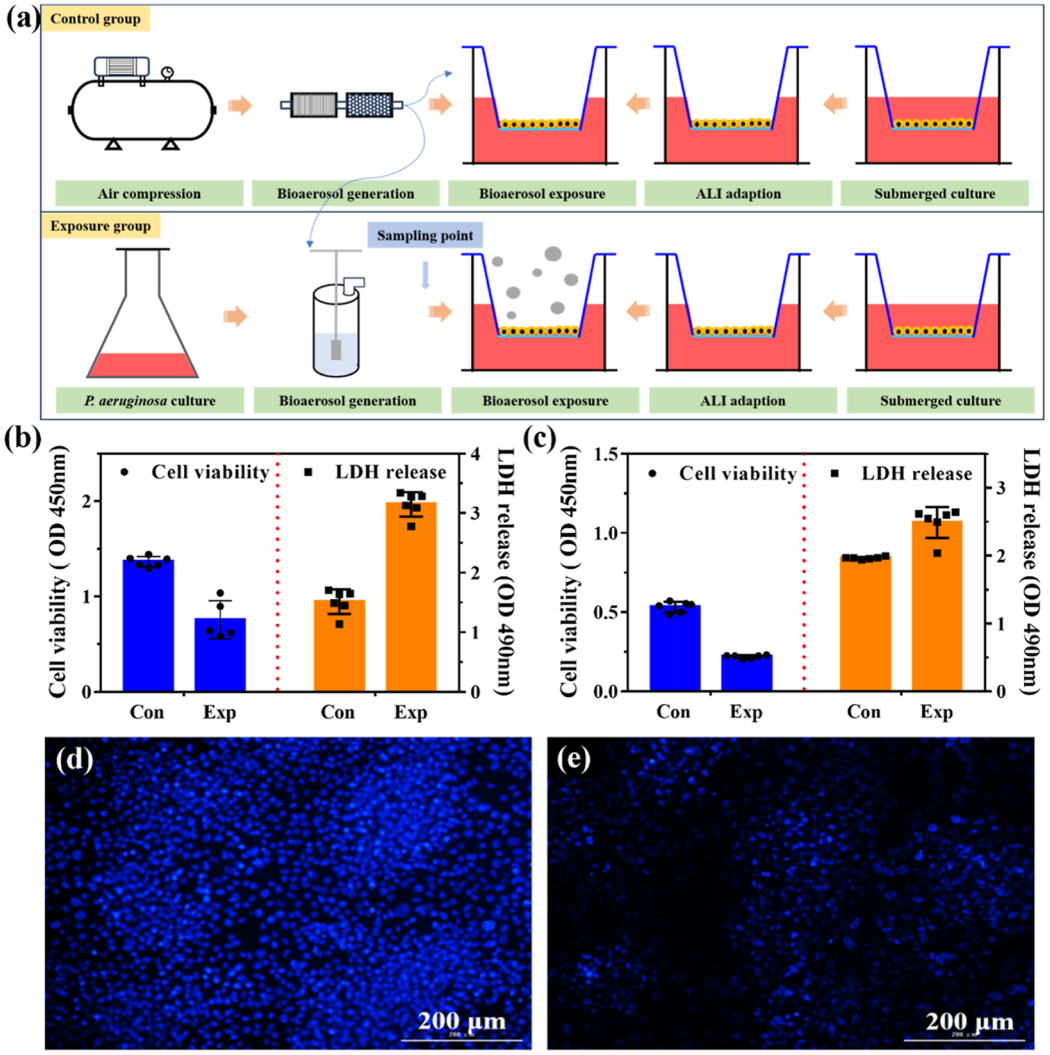

Figure 1. Experimental design and cytotoxicity of *P. aeruginosa* bioaerosol in 16HBE cells. (a) Schematic of the ALI cell model establishment and bioaerosol exposure protocol. (b) Cell viability (CCK-8) and membrane integrity (lactose dehydrogenase (LDH) release) of 16HBE cells after clean air control (Con) or *P. aeruginosa* bioaerosol (Exp) exposure. (c) Normalized cell viability and membrane integrity of 16HBE cells (% of clean air control) after clean air control (Con) or *P. aeruginosa* bioaerosol (Exp) exposure. (d,e) Nuclear morphology (DAPI staining) of 16HBE cells after exposure to clean air (d) or *P. aeruginosa* bioaerosol (e). All cytotoxicity assays were based on three biological replicates, with two technical replicates.

exposure system to quantify the cytotoxicity of *P. aeruginosa* bioaerosol at environmentally relevant concentrations, enabling the direct delivery of aerosolized pathogens to epithelial cells under ALI conditions.

Moreover, cell model selection is another critical factor influencing the accuracy of *in vitro* exposure systems.[20] The immortalized cell lines offer unlimited proliferation and minimal interbatch variability, but they undergo genetic modification during immortalization, significantly compromising their physiological relevance.[21,22] In contrast, primary cells are considered more physiologically relevant,[23] yet their application in health risk assessment is limited due to donor variability and finite lifespan. The effects of reduced physiological relevance in immortalized cells on their performance in exposure systems and the mechanisms by which cell models impact exposure outcomes remain unclear. Therefore, a systematic comparison of cytotoxic responses between primary and immortalized respiratory epithelial cells is necessary to enhance the reliability of the exposure systems.

Therefore, this study established an ALI exposure system to assess the health risks posed by *P. aeruginosa* bioaerosol at environmentally relevant concentrations to respiratory epithelial cells. Cytotoxicity and immune responses to *P. aeruginosa* bioaerosol were compared between immortalized human bronchial epithelial (16HBE) cells and primary normal human bronchial epithelial (NHBE) cells. Additionally, cellular functional differences between these two cell models were investigated through transcriptomic profiling and phenotypic validation. This research elucidated the limitations of immortalized cell lines in cytotoxicity assessment of bioaerosols, optimized cell model selection strategies, and improved the accuracy of health risk assessment systems.

2. MATERIALS AND METHODS

2.1. Reagents and Chemicals

Reagents and chemicals used in this study are detailed in Text S1.

https://doi.org/10.1021/acsestair.5c00326
ACS EST Air XXXX, XXX, XXX−XXX

2.2. Bioaerosol Exposure Experiments

2.2.1. Setup of the Exposure System. The *in vitro* exposure system was set up using a 3-jet Collison nebulizer (BGI, USA), a Woulff bottle, a dryer (Huifen, China), and a CULTEX Radial Flow System (Cultex, Germany). All components were interconnected via a low-adsorption polytetrafluoroethylene pipeline. A comprehensive description of the exposure system is provided in Text S2.

2.2.2. Cell Culture and Cell Model Establishment. The simian virus 40 (SV40)-immortalized 16HBE cells were obtained from the Chinese Academy of Cell Resource Center (Shanghai, China) and cultured in Dulbecco's Modified Eagle's Medium (DMEM). NHBE cells were acquired from Procell Life Science & Technology Co., Ltd. (Wuhan, China) and cultured in the specialized CM-H009 medium. The NHBE cells were isolated from a single adult male donor using enzymatic digestion and mechanical scraping, expanded in specialized bronchial epithelial growth medium, and verified as epithelial cells by pan-cytokeratin immunofluorescence staining. Both media were supplemented with 10% fetal bovine serum (FBS), 100 μg/mL streptomycin, and 100 U/mL penicillin. Cells at passages 3−10 were used to establish the cell model.

For cell model establishment, NHBE and 16HBE cells were seeded at a density of 30000 cells per Transwell insert and cultured under submerged conditions at 37 °C with 5% CO_2. The culture media were refreshed every 48 h (0.5 mL apically and 1.0 mL basally). Once the cell confluence reached 80%, the apical medium was removed to form the ALI 24 h prior to exposure. Both cell models were transferred to the CULTEX Radial Flow System for controlled exposure to bioaerosols.

2.2.3. Bioaerosol Generation and Exposure Procedure. *P. aeruginosa* in the exponential growth phase was harvested by centrifugation at 6000*g* and resuspended in phosphate buffer saline (PBS) to a final concentration of 5×10^6 CFU/mL. The suspension was aerosolized at a flow rate of 6.0 L/min using a nebulizer. The bioaerosol was maintained at 90%−95% relative humidity using a dryer system and delivered to cellular exposure models at 5.0 mL/min. Based on pilot experiments, filtered clean air served as the control. Details are provided in Text S3 and Figure S1. The bioaerosol was collected using an SKC BioSampler (SKC, USA) positioned upstream of the exposure chamber and subsequently quantified by gradient dilution and culture-based enumeration. The delivered *P. aeruginosa* aerosol concentration was $(1.0 \pm 0.3) \times 10^5$ CFU/m^3. The particle size of generated bioaerosols was maintained at approximately 1−3 μm.[24] The cell models were incubated in DMEM supplemented with 1% FBS at 37 °C throughout the 3 h exposure period. After exposure, cells were transferred to fresh medium in new 12-well plates and cultured for an additional 12 h prior to analysis. The detail on exposure experimental design is illustrated in Figure 1a.

2.3. Cytotoxicity Assays

Cytotoxicity induced by *P. aeruginosa* bioaerosol was evaluated based on cell viability, cell membrane permeability, and nuclear morphology analyses. Cell viability was evaluated using the Cell Counting Kit-8 (CCK-8). Cell membrane permeability was determined using the Cytotoxicity LDH Assay Kit-WST, by measuring LDH activity in the culture medium. Nuclear morphology was assessed by staining with 4′,6-diamidino-2-phenylindole (DAPI). Detail methods for cytotoxicity assays are provided in Text S4.

2.4. Transcriptome Analysis

Total RNA was extracted from NHBE and 16HBE cells following exposure to *P. aeruginosa* bioaerosol or clean air using the Total RNA Extractor Kit. Poly(A)$^+$ mRNA was isolated via oligo(dT) magnetic beads followed by double-stranded cDNA synthesis. Sequencing libraries were quantified with a Qubit 4.0 Fluorometer (Thermo, USA) and sequenced on an Illumina NovaSeq X Plus system (Illumina, USA) with the NovaSeq Reagent Kit. Gene expression levels were normalized as transcripts per million (TPM), followed by a $\log_{10}$ (TPM +1) transformation for variance stabilization. Differential expression analysis was performed with DESeq2, and differentially expressed genes (DEGs) were defined as $|\log_2 FC| \geq 1$ and p-adjust < 0.05. Kyoto Encyclopedia of Genes and Genomes (KEGG) pathway enrichment analysis was conducted on the identified DEGs.

2.5. Phenotypic Validation

Phenotypic experiments were conducted to validate the proliferation and adhesion properties of the two cell models. Cellular proliferative capacity was characterized by morphological observation and cell viability assays. Adhesion capability was evaluated based on cellular morphology, junctional protein expression, and barrier permeability. The morphology of NHBE and 16HBE cells was characterized using scanning electron microscopy (SEM, Hitachi, Japan). Junctional protein expression was analyzed by quantitative reverse transcription PCR (qRT-PCR), and the barrier permeability of the cell models was assessed with 4 kDa fluorescein isothiocyanate-dextran. Detail methods of phenotypic validation are provided in Text S5. The primers used in this study are provided in Table S1 sourced from Primer Bank (https://pga.mgh.harvard.edu/primerbank/).

2.6. Statistical Analyses

Graphical presentation and statistical analyses were carried out using GraphPad Prism software. The two-way ANOVA or t-test was employed to identify significant differences between exposure and control groups, as appropriate. All statistical analyses were based on three biological replicates. Within each experiment, technical replicates (e.g., duplicate wells for CCK-8, LDH, epithelial barrier permeability, and qRT-PCR assays) were included. For RNA-seq, although the study included three biological replicates without technical replicates, all samples underwent rigorous quality control. p-values < 0.05 was considered statistically significant.

3. RESULTS AND DISCUSSION

3.1. Cytotoxicity of *P. aeruginosa* Bioaerosol to 16HBE Cells

This study established an ALI exposure system to deliver environmentally relevant concentrations of *P. aeruginosa* bioaerosol to both primary and immortalized respiratory epithelial cells, thereby minimizing limitations of conventional submerged exposure systems. The exposure concentration of $(1.0 \pm 0.3) \times 10^5$ CFU/m^3 simulated an environmentally relevant level capable of inducing cytotoxicity (Figure S1).[25] Compared to the clean air control, exposure to *P. aeruginosa* bioaerosol significantly reduced 16HBE cell viability to 56.2% ± 14.9% and increased LDH release by (2.1 ± 0.1)-fold (Figure 1b,c), indicating substantial cellular damage. These findings were further corroborated by DAPI staining, which revealed DNA fragmentation and pyknosis in cells exposed to *P. aeruginosa* bioaerosol (Figure 1e). Quantitative analysis showed a 43.2% reduction in DAPI fluorescence intensity in 16HBE cells exposed to bioaerosol (Figure 1d,e). Collectively, these end points, including cell viability, LDH release, and nuclear damage, demonstrated the cytotoxic potential of *P. aeruginosa* bioaerosol, aligning with effects observed in conventional submerged exposure systems.[12] In this study, we used CFU as a simplified and widely accepted dosimetry metric. However, bacteria may undergo viability reduction, structural damage, and phenotypic alteration during nebulization and drying.[26] CFU-based quantification overlooks nonviable components, such as bacterial debris, endotoxins, and extracellular DNA, which can contribute to cytotoxicity. Thus, reliance on CFU may underestimate the total bioactive burden, potentially leading to an overestimation of the contribution of viable bacteria to the observed cytotoxicity.

https://doi.org/10.1021/acsestair.5c00326
ACS EST Air XXXX, XXX, XXX−XXX

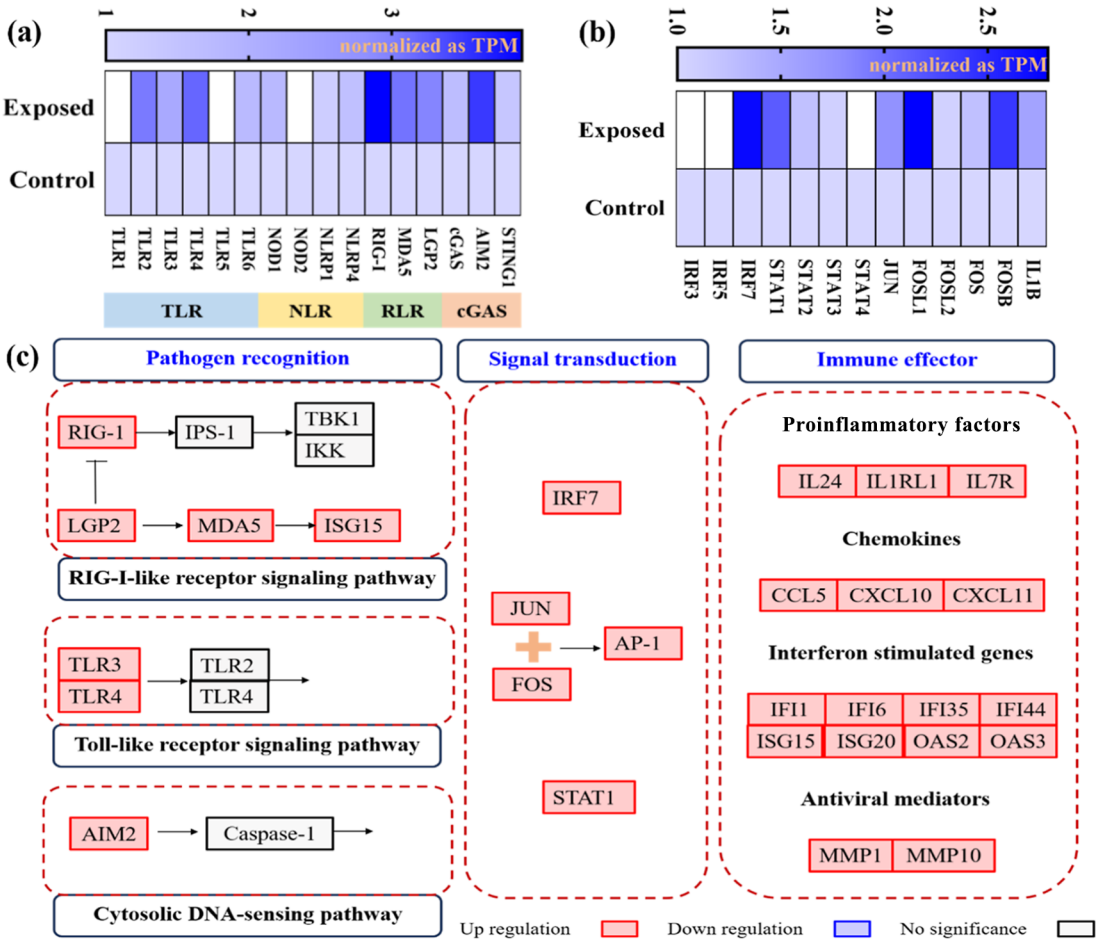

Figure 2. Transcriptome profiling and immune response of 16HBE cells exposed to *P. aeruginosa* bioaerosol. (a) Expression levels of key PRR genes after clean air or *P. aeruginosa* bioaerosol exposure. (b) Expression levels of essential transcription factor genes after clean air or *P. aeruginosa* bioaerosol exposure. In (a,b), white boxes denote downregulated genes, and the blue gradient (light to dark) represents increasing upregulation. (c) Immune response of 16HBE cells to *P. aeruginosa* aerosol, illustrating representative genes involved in pathogen recognition, signal transduction, and immune effector responses. RNA-seq analysis was based on three biological replicates (no technical replicates). Gene expressions were normalized as TPM.

3.2. Cellular Responses of 16HBE Cells to *P. aeruginosa* Bioaerosol Exposure

3.2.1. Pathway Enrichment Analysis of DEGs in 16HBE Cells Induced by *P. aeruginosa* Bioaerosol Exposure. To identify the key regulatory pathways mediating 16HBE cellular response to *P. aeruginosa* bioaerosol, transcriptome profiling was performed. Bioaerosol exposure resulted in 127 DEGs in 16HBE cells out of a total of 62,703 genes passing quality filters, of which 37 were downregulated and 90 were upregulated (Figure S2). KEGG pathway enrichment analysis identified 15 significantly enriched pathways, which were categorized into two major biological themes: infectious diseases (7 pathways) and the immune system (6 pathways) (Figure S3). This transcriptomic signature indicated that *P. aeruginosa* bioaerosol exposure triggered cascades associated with pathogen infection and immune activation in 16HBE cells.

The significantly enriched infectious disease related pathways included influenza A, hepatitis C, coronavirus disease, Epstein−Barr virus infection, hepatitis B, measles, and Kaposi sarcoma-associated herpesvirus infection (Figure S3). However, the immortalized 16HBE cell line exhibited distinct activation of viral infection-related pathways compared to primary bronchial epithelial cells.[27] This immortalization-associated background signaling may confound the interpretation of bacterial response specific enrichment, potentially leading to inaccurate attribution of the infection-related pathway. Consequently, we prioritized the analysis of conserved immune system pathways.

Specifically, *P. aeruginosa* bioaerosol exposure induced significantly enrichment of immune related pathways in 16HBE cells, including RIG-like receptor (RLR), NOD-like receptor (NLR), toll-like receptor (TLR), cytosolic DNA-sensing (cGAS-STING) signaling pathways, interleukin 17 (IL-17), and chemokine signaling pathways (Figure 2a). The RLR, NLR, TLR, and cGAS-STING pathways constituted the core network of pattern recognition receptors (PRRs) in the innate immune system. These receptors recognized pathogen-associated molecular patterns (PAMPs) through structural complementarity, thereby triggering downstream immune cascades.[28] Activation of conserved PRR pathways by *P. aeruginosa* has been extensively documented in conventional submerged exposure models.[29] These activation patterns also were observed under the ALI exposure conditions. Downstream, IL-17, and chemokine signaling mainly mediate inflammatory amplification: IL-17 signaling induces pro-inflammatory cytokines and maintains epithelial barrier

https://doi.org/10.1021/acsestair.5c00326
ACS EST Air XXXX, XXX, XXX−XXX

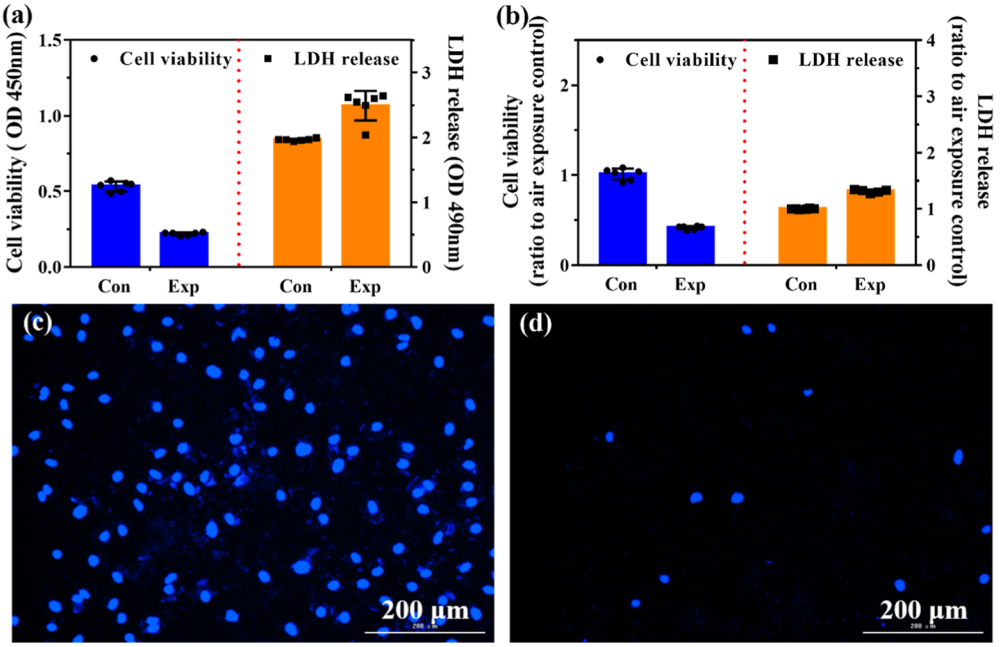

Figure 3. Cytotoxicity of *P. aeruginosa* bioaerosol in NHBE cells. (a) Cell viability (CCK-8) and membrane integrity (LDH release) of NHBE cells after clean air control (Con) or *P. aeruginosa* bioaerosol (Exp) exposure. (b) Normalized cell viability and membrane integrity of NHBE cells (% of clean air control) after clean air control (Con) or *P. aeruginosa* bioaerosol (Exp) exposure. (c,d) Nuclear morphology (DAPI staining) of NHBE cells after exposure to clean air (c) or *P. aeruginosa* bioaerosol (d). All cytotoxicity assays were based on three biological replicates, with two technical replicates.

integrity; chemokine signaling regulates immune cell migration and amplifies the inflammatory response.[30] Transcriptomic analysis revealed that 16HBE cells mount a defense against *P. aeruginosa* bioaerosol through PRR-driven pathogen recognition, coupled with IL-17 and chemokine-mediated inflammatory amplification.

3.2.2. Defense Mechanisms of 16HBE Cells against *P. aeruginosa* Bioaerosol. To elucidate the response mechanisms of 16HBE cells to *P. aeruginosa* bioaerosol exposure, the expression profiles of core genes in PRR pathways was quantified using the relative TPM ratios (bioaerosol exposure vs control air control) based on transcriptome sequencing data. As shown in Figure 2a, bioaerosol exposure significantly upregulated the expression of key PRRs, including: TLR 4 (*TLR4*, p = 0.02), TLR 6 (*TLR6*, p = 0.04), retinoic acid-inducible gene-I (*RIG-I*, p = 0.02), melanoma differentiation-associated gene 5 (*MDA5*, p = 0.03), laboratory of genetics and physiology 2 (*LGP2*, p = 0.04), absent in melanoma 2 (*AIM2*, p = 0.01), stimulator of interferon gene (*STING*, p = 0.04). Notably, while all of these PRR pathways (NLR, TLR, RLR, and cGAS-STING) were significantly enriched in 16HBE cells after *P. aeruginosa* bioaerosol exposure, no DEGs were detected among NLRs. Induction of downstream effector activator protein 1 (AP-1) confirms functional NLR pathway activation. The RLRs (*RIG-I*, *MDA5*, *LGP2*) were identified as DEGs, suggesting that the RLR pathway may dominate the host response to *P. aeruginosa* infection.

As reported, the function of PRRs acts as sentinels of innate immunity in barrier epithelial. Upon recognizing the PAMPs, PRRs trigger the downstream signaling cascades that activate transcriptional regulators, the core effectors of immune gene expression.[31] In the 16HBE cells, *P. aeruginosa* bioaerosol exposure significantly upregulated the transcription factor genes, including interferon regulatory factor 7 (*IRF7*), AP-1 (a heterodimeric complex composed of FOS and JUN family), and signal transducer and activator of transcription 1 (*STAT1*) (Figure 2b). Protein−protein interaction (PPI) network analysis of DEGs via STRING confirmed the key role of STAT1 and IRF7 in the immune response of 16HBE cells (Figure S4). These transcription factors formed dense interaction hubs with chemokines (e.g., C-X-C Motif Chemokine Ligand 11, *CXCL11*; C-X-C Motif Chemokine Ligand 10, *CXCL10*; C−C Motif Chemokine Ligand 5, *CCL5*), interferon-stimulated genes (*ISGs*), and other immune mediators, orchestrating a coordinated defense program (Figure S4).

Based on the regulatory network analysis of DEGs, a three-phase response mechanism of 16HBE cells to *P. aeruginosa* was proposed, as shown in Figure 2c. (1) Recognition phase: PAMPs of *P. aeruginosa* engage host PRRs, predominantly activating the RLR, TLR, NLR, and cGAS-STING pathways; (2) signal transduction phase: activated PRRs trigger the signaling cascades, leading to activation of transcription factors, including IRF7, AP-1, and STAT1; (3) immune effector phase: activated transcription factors orchestrate a comprehensive immune response. Specifically, STAT1 and IRF7 induced the expression of *ISGs*. AP-1 mediated the secretion of pro-inflammatory cytokines and matrix metallopeptidase (MMPs). Our analysis revealed how *P. aeruginosa* bioaerosol modulates respiratory epithelia cell responses through PRR-driven transcription activation.

3.3. Cytotoxicity of *P. aeruginosa* Bioaerosol to NHBE Cells

Given the superior physiological relevance of the primary cells, the cytotoxic effects and immune responses of the bioaerosol on primary NHBE cells were assessed in comparison with the immortalized 16HBE cell line. As shown in Figure 3a,b, exposure to *P. aeruginosa* bioaerosol significantly reduced the cell viability of the NHBE cells by 58.3% ± 1.4% and increased LDH release (1.3 ± 0.1)-fold. DAPI imaging further confirmed

https://doi.org/10.1021/acsestair.5c00326
ACS EST Air XXXX, XXX, XXX−XXX

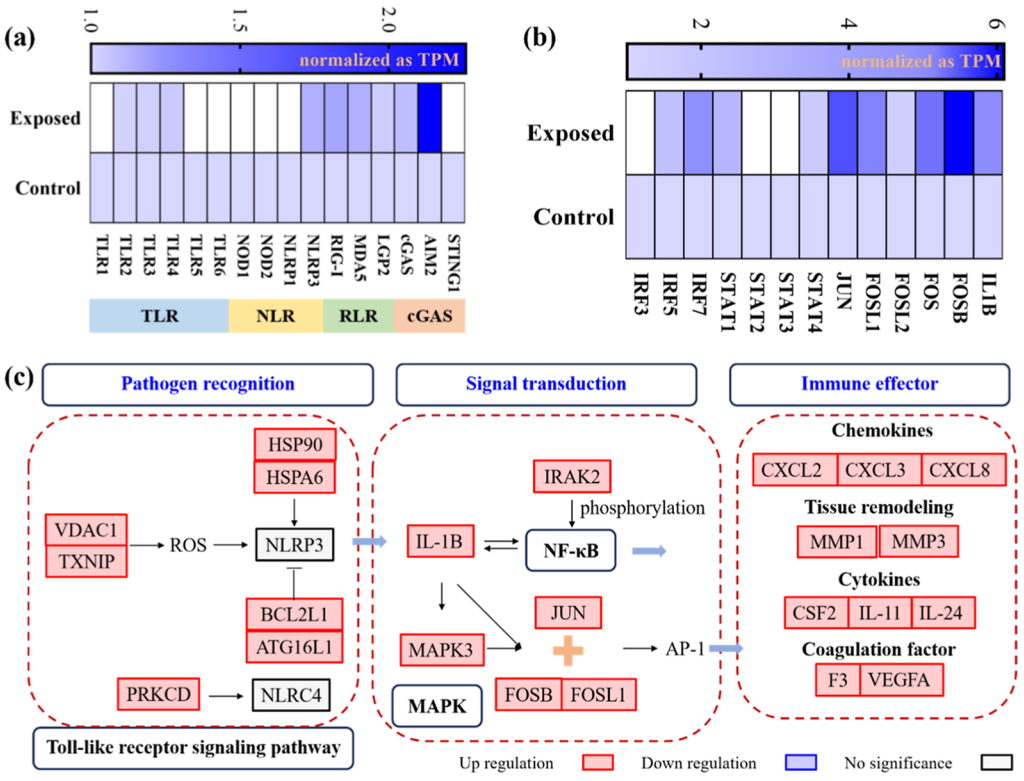

Figure 4. Transcriptome profiling and immune response of NHBE cells to *P. aeruginosa* bioaerosol. (a) Expression levels of key PRR genes after clean air of *P. aeruginosa* bioaerosol exposure. (b) Expression levels of essential transcription factor genes after clean air or *P. aeruginosa* bioaerosol exposure. In (a,b), white boxes denote downregulated genes, and the blue gradient (light to dark) represents increasing upregulation. (c) Immune response of NHBE cells to *P. aeruginosa* bioaerosol, illustrating representative genes involved in pathogen recognition, signal transduction, and immune effector responses. RNA-seq analysis was based on three biological replicates (no technical replicates). Gene expressions were normalized as TPM.

these effects: compared to the nuclear fluorescence in clean air control, *P. aeruginosa* bioaerosol exposure resulted in 76.3% reduction in fluorescence intensity with characteristic apoptotic morphology (Figure 3c,d).

Compared to the 16HBE cell line, which showed only a 43.8% decrease in cell viability and a 2.1-fold increase in LDH release, the NHBE cell line exhibited lower sensitivity to *P. aeruginosa* bioaerosol exposure. A two-way ANOVA with cell type (NHBE vs 16HBE) and exposure condition (clean air vs *P. aeruginosa* bioaerosol) as fixed factors revealed a highly significant interaction for LDH release (interaction $p < 0.001$), indicating that the two cell models exhibited divergent biological responses to the bioaerosol. Despite higher proliferative capacity, immortalized 16HBE cells are more susceptible to bioaerosol-induced cytotoxicity, whereas primary NHBE cells exhibit greater resilience.

3.4. Cellular Responses of NHBE Cells to *P. aeruginosa* Bioaerosol Exposure

3.4.1. Pathway Enrichment Analysis of DEGs in NHBE Cells Induced by *P. aeruginosa* Bioaerosol Exposure. Transcriptome profiling was comparatively performed on the NHBE cells to delineate their response profiles to *P. aeruginosa* bioaerosol exposure. As shown in Figure S5, *P. aeruginosa* bioaerosol exposure induced 156 DEGs in the NHBE cells identified from 62,703 genes that passed the quality filters, comprising 81 downregulated and 75 upregulated genes. KEGG enrichment analysis identified 20 significantly enriched pathways (Figure S6), 6 of which were shared with the 16HBE cells. The commonly enriched pathways were IL-17 signaling pathway, AGE-RAGE signaling pathway in diabetic complications, Kaposi sarcoma-associated herpesvirus infection, Coronavirus disease (COVID-19), viral protein interaction with cytokine and cytokine receptor, and NLR signaling pathway. This shared pathway enrichment indicates that the core immune pathways against *P. aeruginosa* are functionally conserved between the NHBE and 16HBE cell lines.

Notably, NHBE cells exhibited unique significant enrichment in five critical signal transduction pathways (Figure S6), including tumor necrosis factor (TNF), mitogen-activated protein kinase (MAPK), wingless/integrated (Wnt), nuclear factor kappa-light-chain-enhancer of activated B cells (NF-κB), and transforming growth factor beta (TGF-β) signaling pathways. Functionally, these pathways form a coordinated defense network. The TNF/MAPK/NF-κB axis drives rapid pathogen clearance through inflammatory activation, directly accounting for observed cytotoxicity.[32] However, the TGF-β/Wnt axis provides negative feedback by suppressing inflammatory signals and promoting epithelial repair, playing a core anti-inflammatory function.[33] Activation of these pathways enabled the NHBE cells to mount a coordinated immune response against *P. aeruginosa* bioaerosol.

Innate immune defenses comprise pathogen recognition, signal transduction, and immune effector activation.[34] In this study, cell-type-specific differences were observed in the responses of NHBE and 16HBE cells to *P. aeruginosa* bioaerosol exposure. In NHBE cells, only NLR pathway enrichment reached statistical significance (Figure S6), but the TLR, RLR, and cGAS-STING pathways exhibited non-

https://doi.org/10.1021/acsestair.5c00326
ACS EST Air XXXX, XXX, XXX−XXX

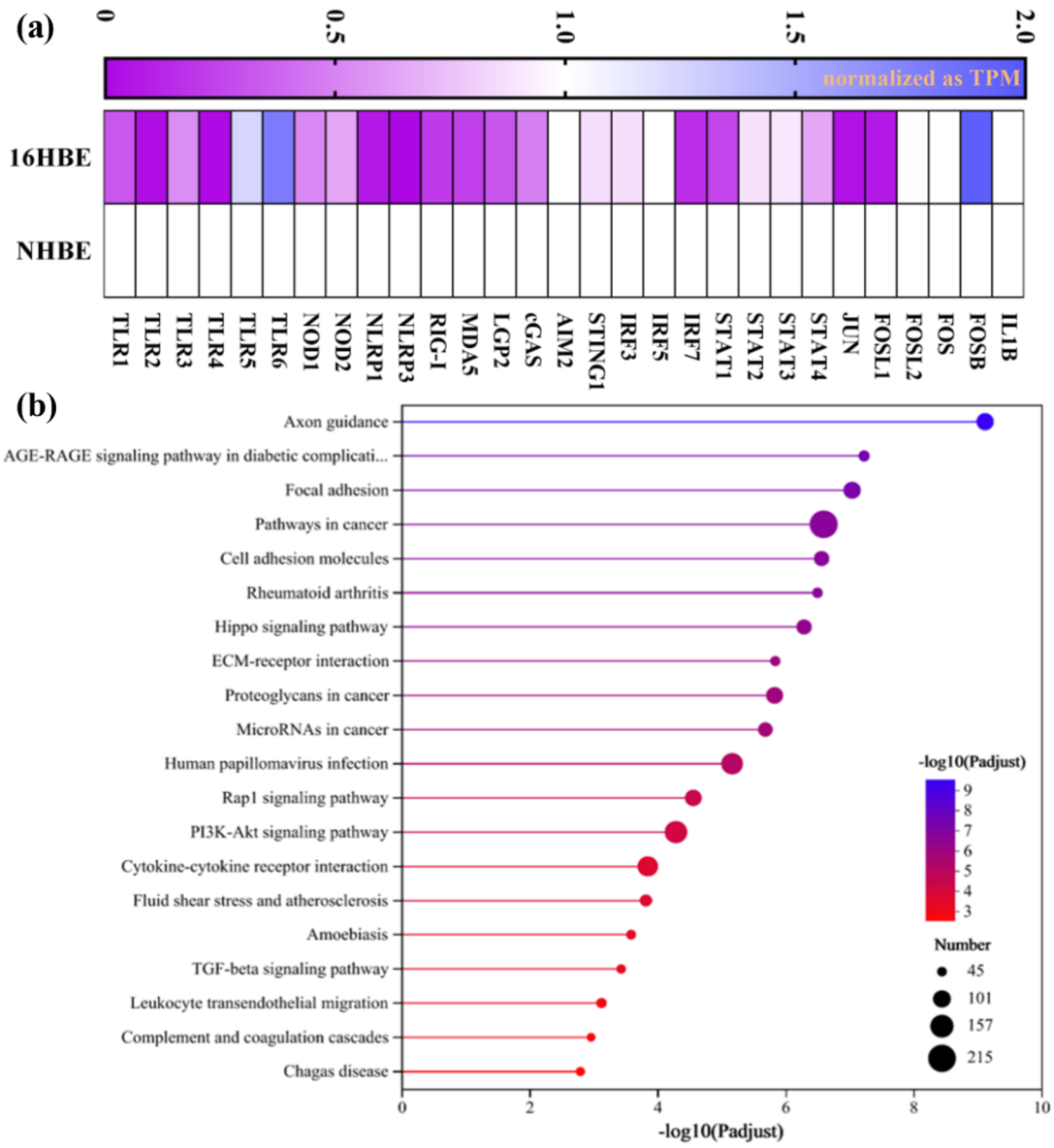

Figure 5. Comparative transcriptomic profiling of 16HBE and NHBE cells under clean air control. (a) Expression levels of core PRR pathway components, including receptors and key transcription factors, in 16HBE and NHBE cells under clean air control. RNA-seq analysis was based on three biological replicates (no technical replicates). (b) KEGG pathway enrichment of DEGs in 16HBE and NHBE cells under clean air control. Gene expressions were normalized as TPM.

significant enrichment (adjusted p values: TLR = 0.1; RLR = 0.5; cGAS-STING = 0.5). NLR priming activated comprehensive signal transduction, the TNF/MAPK/NF-κB axis amplified inflammation, and TGF-β/Wnt axis mediated damage control. In contrast, 16HBE cells exhibited significant enrichment of multiple PRR pathways, including RLR, NLR, TLR, and cGAS-STING in response to *P. aeruginosa* bioaerosol. The PRR activation directly triggered transcription factor expression without downstream signal transduction activation. This functional divergence underscored the complete defense program of the NHBE cells from pathogen recognition to inflammatory resolution, enabling a coordinated antimicrobial response. While in 16HBE cells, incomplete pathway crosstalk limited inflammatory resolution, resulting in an incomplete immune response. Therefore, reliance on 16HBE cells alone may underestimate the cytotoxicity of *P. aeruginosa* bioaerosol exposure.

3.4.2. Defense Mechanism of the NHBE Cells against *P. aeruginosa* Bioaerosol. Similar to observations in 16HBE cells, *P. aeruginosa* bioaerosol exposure resulted in enrichment of the NLR signaling pathway without differential expression of key NLR genes in NHBE cells (Figure 4a). Upon activation, NLR inflammasomes cleave the pro-IL-1β precursor to release mature interleukin-1beta (IL-1β), amplifies NF-κB, and MAPK signaling.[35] The significant upregulation of downstream effector molecules (e.g., IL-1β, AP-1 subunits) directly reflects the functional activation of the NLR pathway (Figure 4b).

IL-1β served as the core inflammatory trigger, initiating a signaling cascade that induced the expression of chemokines, MMPs, and transcription factor AP-1 (Figure 4b). AP-1 mediated transcription of immune effectors, including pro-inflammatory cytokines, MMPs, and angiogenic factors. PPI network analysis of DEGs in NHBE cells exposed to *P. aeruginosa* bioaerosol highlighted the central role of AP-1 and

https://doi.org/10.1021/acsestair.5c00326
ACS EST Air XXXX, XXX, XXX−XXX

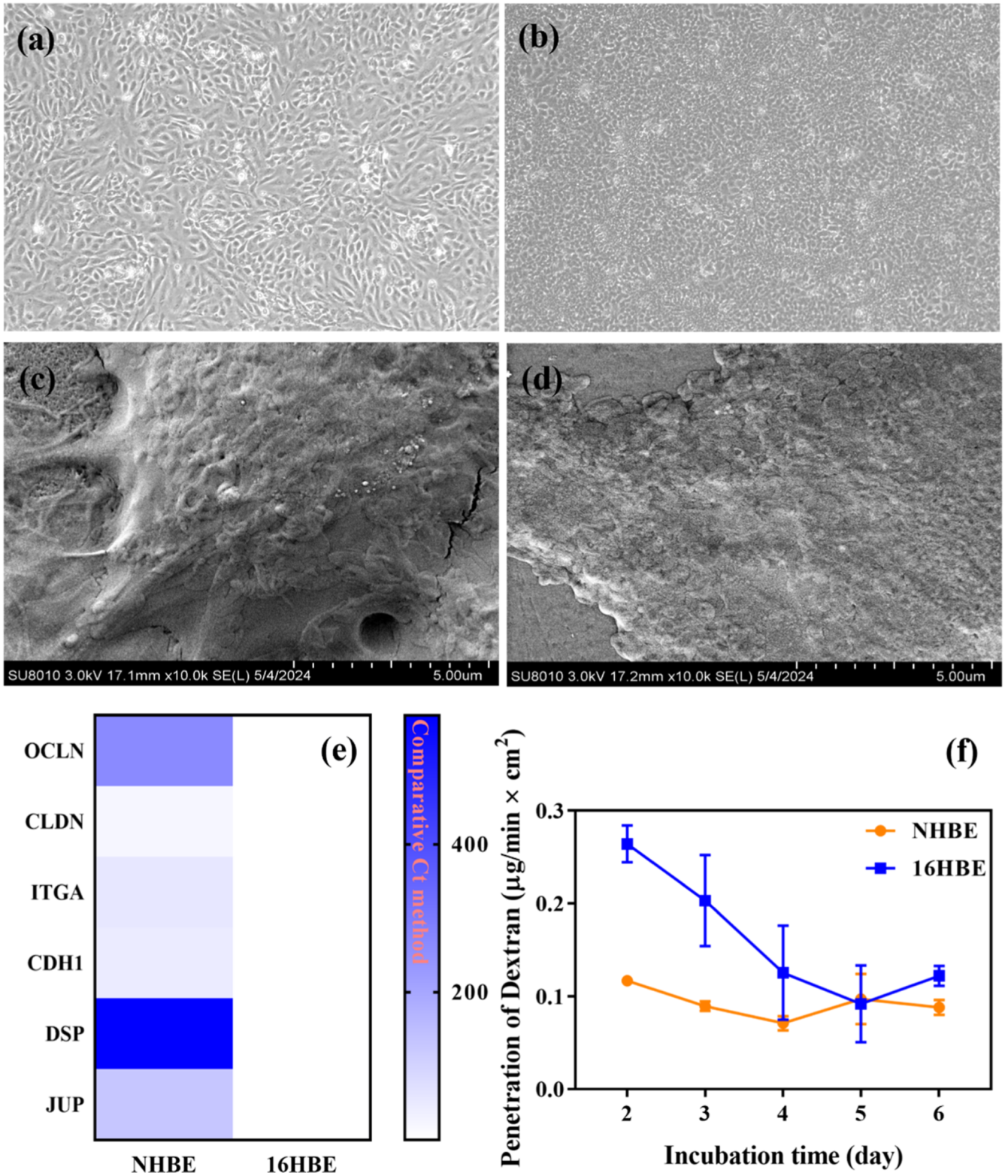

Figure 6. Phenotypic validation of differential function between 16HBE cells and NHBE cells exposed to clean air control. (a,b) Microscopic imaging of NHBE cells (a) and 16HBE cells (b). (c,d) SEM imaging of NHBE cells (c) and 16HBE cells (d). (e) The relative expression levels of key adhesion molecules between 16HBE and NHBE cells. Gene expression was quantified using the comparative Ct method ($2^{-\Delta\Delta Ct}$). (f) The permeability of epithelial barrier in 16HBE and NHBE cell models. Phenotypic validation assays were based on three biological replicates, with two technical replicates.

IL-1β (Figure S7). IL-1β acted as the primary inflammatory initiator, while AP-1 functioned as its key downstream executor. Their synergy amplified the expression of pro-inflammatory cytokines, chemokines, and tissue-remodeling enzymes, thereby exacerbating the inflammatory response.

https://doi.org/10.1021/acsestair.5c00326
ACS EST Air XXXX, XXX, XXX−XXX

The defense mechanism of NHBE cells against the *P. aeruginosa* bioaerosol is summarized in Figure 4c. (1) Recognition phase: NLR served as the primary PRR for *P. aeruginosa* detection; (2) signal transduction phase: NLR signaling activated the MAPK/NF-κB pathway via IL-1β, thereby enhancing AP-1 activity; (3) immune effector phase: IL-1β and AP-1 synergistically amplified the expression of pro-inflammatory cytokines, chemokines, and tissue-remodeling enzymes. Exposure to bioaerosol induced transcriptomic reprogramming, which in turn led to reduced cell viability and compromised membrane integrity.

Notably, 16HBE and NHBE cells exhibited distinct immune responses to *P. aeruginosa* exposure. Specifically, the 16HBE cells primarily utilized RLR, TLR, NLR, and cGAS-STING pathways to recognize *P. aeruginosa* bioaerosol and subsequently activated the transcription factors IRF7 and AP-1 to modulate immune responses. In contrast, NHBE cells relied more on the NLR pathway for *P. aeruginosa* recognition, with IL-1β and AP-1 playing a central role in downstream gene expression. That is, distinct cell types employ divergent recognition strategies. Further studies are needed to elucidate the cell-type-specific recognition preference and uncover the mechanisms underlying the differential responses to *P. aeruginosa* exposure, ultimately promoting the selection of optimal cell exposure systems.

3.5. Inherent Disparities between 16HBE and NHBE Cells Shaped Their Differential Immune Responses

To elucidate the basis for differential cytotoxicity responses, a comparative transcriptomic analysis was conducted between NHBE and 16HBE cells under clean air control exposure. As shown in Figure S8, there were 7767 DEGs obtained, 3883 upregulated and 3884 downregulated genes. This intercellular difference vastly exceeded the transcriptional changes induced by *P. aeruginosa* bioaerosol exposure (127 DEGs in 16HBE; 156 DEGs in NHBE). Principal component analysis (PCA) and Pearson correlation analysis collectively demonstrated profound transcriptomic divergence between NHBE and 16HBE cells. PCA showed that intercell-type separation (NHBE vs 16HBE) dominated over intracell-type variation (bioaerosol vs clean air), with the first principal component accounting for 81.4% of the total variance (Figure S9). Pearson correlation between cell types were moderate (r = 0.86−0.89), whereas within each cell type, correlations approached perfection (r = 0.99−1.00) (Figure S10). The divergence strongly challenges the suitability of 16HBE cells for bioaerosol risk assessment.

KEGG enrichment analysis of DEGs between NHBE and 16HBE cells identified 62 significantly enriched pathways. The top 20 were clustered into two major functional themes: dysregulation of cell adhesion and migration, and activation of oncogenic signaling (Figure 5a), universal features induced by immortalization.[36] This enrichment profile suggested a functional divergence between the 16HBE and NHBE cells.

Phenotypic characterization confirmed fundamental differences in the proliferation and adhesion between NHBE and 16HBE cells. NHBE cells exhibited 39.2% lower cell viability than 16HBE cells at identical seeding densities (Figures 1b and 3a). NHBE cell cultures entered senescence by passages 5−8, whereas 16HBE cells maintained sustained proliferative capacity. Morphologically, NHBE cells exhibited typical epithelial polygonal morphology and formed contact-inhibited monolayers (Figure 6a), while 16HBE cells displayed pebble-like morphology with multilayer growth (Figure 6b). These observations highlight the finite replicative capacity of NHBE cells and the enhanced proliferative potential of 16HBE cells.

Adhesion dysregulation in 16HBE cells was demonstrated by SEM morphology, junction protein expression, and barrier function. For SEM morphological analysis, NHBE cells formed continuous monolayers with extensive lamellar pseudopodia, while 16HBE exhibited fragmented adhesion with sparse pseudopodia (Figures 6c,d). qRT-PCR analysis showed significantly higher expression of key adhesion molecules in the NHBE cells. Specifically, the relative expression levels of key adhesion molecules in NHBE cells were 255.4 ± 31.2 (*OCLN*), 20.6 ± 1.8 (*CLDN*), 52.9 ± 3.3 (*ITGA*), 42.5 ± 10.1 (*CDH1*), 577.0 ± 118.4 (*DSP*), and 163.2 ± 56.8 (*JUP*)-fold relative to 16HBE cells (Figure 6e). Barrier integrity was markedly stronger in NHBE monolayers, as indicated by significantly lower dextran permeability than 16HBE cells (p < 0.01), correlating with junction protein levels (Figure 6f). This triad of evidence confirmed reduced cell adhesion in 16HBE cells.

Divergence in proliferation and adhesion constituted the core fundamental differences between 16HBE and NHBE cell lines, which likely affect the pathogen recognition to *P. aeruginosa* bioaerosol. Transcriptome analysis revealed downregulation of key PRR genes in 16HBE cells compared with NHBE cells under clean air control (Figure 5b), which are aligned with the reported PRR suppression in high-proliferation/low-adhesion cancer cells.[37] The 16HBE cells may require compensatory expression upregulation against pathogen challenge, thereby explaining their exaggerated activation of the PRR pathway.

This study identified a series of associated functional differences between immortalized 16HBE and primary NHBE cells. While 16HBE cells exhibited sustained proliferative capacity compared to NHBE cells, cellular immortalization was accompanied by adhesion dysregulation and PRR signaling downregulation, which coincided with divergent cytotoxic responses to *P. aeruginosa* bioaerosol exposure. Upon *P. aeruginosa* bioaerosol exposure, NHBE cells displayed a comprehensive immune response, whereas 16HBE cells showed compensatively upregulated PRR signaling, resulting in a reduced direct cytotoxicity. These differences in gene expression patterns were correlated with distinct cytotoxicity profiles in the two cell models.

4. CONCLUSION

This study established an ALI exposure system to deliver *P. aeruginosa* bioaerosol at environmentally relevant concentrations to immortalized 16HBE and primary NHBE cells. Cytotoxicity and transcriptome profiling revealed divergent responses between the two cell models. Immortalized 16HBE cells were more susceptible to bioaerosol-induced cytotoxicity, whereas primary NHBE cells exhibited greater resilience. Transcriptome analysis indicated that 16HBE cells primarily utilized RLR, TLR, NLR, and cGAS-STING pathways to sense *P. aeruginosa* bioaerosol, subsequently activating transcription factors IRF7 and AP-1 to modulate immune responses. In contrast, the NHBE cells relied more on NLR, with IL-1β and AP-1 playing a central role in the downstream gene regulation. Comparative analysis under clean air control conditions identified substantial differences between the two cell models, which may associate with their distinct transcriptional and functional responses to bioaerosol exposure. Notably, 16HBE

https://doi.org/10.1021/acsestair.5c00326
ACS EST Air XXXX, XXX, XXX−XXX

cells demonstrated compensatory hyperactivation of PRRs but impaired barrier integrity and reduced proliferative capacity under stress, whereas NHBE cells mounted a comprehensive immune response concurrent with greater cytotoxicity. These findings highlight that the use of immortalized 16HBE cells alone may not fully recapitulate the responses of primary airway epithelium to *P. aeruginosa* bioaerosol exposure, underscoring the importance of cell model selection in inhalation toxicology.

5. LIMITATION

This study has several important limitations that warrant consideration. The control group was exposed to filtered clean air rather than aerosolized PBS, primarily due to the constraints of exposure system, which could not simultaneously generate both bioaerosol and PBS aerosol. Although PBS aerosol and clean air showed no significant difference in cytotoxicity, the physical effects of PBS droplets could not be ignored. Exposure dose was quantified solely by CFU and overlooked nonviable components. The nebulization and drying process may alter survival rates, structural integrity, and phenotypic properties, thereby influencing host immune responses. Reliance on CFU alone may underestimate the total bioactive burden. Future studies should integrate complementary metrics, including nonviable components. Only one exposure concentration and a fixed exposure duration limited the assessment of dose−response relationships and kinetic dynamics of the host responses. The model lacks key physiological features, such as functional cilia, mucus secretion, and mature barrier function due to the incomplete ALI differentiation. The physiological relevance of this model is limited. However, in comparative studies involving immortalized cell lines, the use of nonfully differentiated cells may be more appropriate to avoid confounding effects arising from divergent differentiation states. Absence of protein-level validation represents an additional limitation as transcriptomic data alone cannot confirm the functional activation of signaling pathways, although some pathways were supported by complementary phenotypic assays. Collectively, these limitations highlight the need for more physiologically relevant and technically matched exposure systems in future bioaerosol research.

■ ASSOCIATED CONTENT

Supporting Information

The Supporting Information is available free of charge at https://pubs.acs.org/doi/10.1021/acsestair.5c00326.

Chemicals and regents used in this study; detail of the exposure system setup; pilot experiments; protocol of cytotoxicity assays used in this study; phenotypic validation assays including morphology of SEM, qRT-PCR, and barrier permeability analysis; primers used in this study; pilot experiments for control group and concentration selection; number of DEGs induced by *P. aeruginosa* bioaerosol exposure in the 16HBE cell model; KEGG pathway enrichment of DEGs induced by *P. aeruginosa* bioaerosol exposure in the 16HBE cell model; PPI network analysis of DEGs induced by *P. aeruginosa* bioaerosol exposure in the 16HBE cell model; number of DEGs induced by *P. aeruginosa* bioaerosol exposure in the NHBE cell model; KEGG pathway enrichment of DEGs induced by *P. aeruginosa* bioaerosol exposure in the NHBE cell model; PPI network analysis of DEGs induced by *P. aeruginosa* bioaerosol exposure in the NHBE cell model; number of DEGs between 16HBE and NHBE cells after exposure to clean air; PCA diagram of RNA sequencing results of different groups; and Pearson correlation matrix plots RNA sequencing results of different groups (PDF)

■ AUTHOR INFORMATION

Corresponding Author

Guiying Li − *Guangdong-Hong Kong-Macao Joint Laboratory for Contaminants Exposure and Health, Guangdong Key Laboratory of Environmental Catalysis and Health Risk Control, Institute of Environmental Health and Pollution Control, Guangdong University of Technology, Guangzhou 510006, China; Guangzhou Key Laboratory of Environmental Catalysis and Pollution Control, Guangdong Basic Research Center of Excellence for Ecological Security and Green Development, School of Environmental Science and Engineering, Guangdong University of Technology, Guangzhou 510006, China;* orcid.org/0000-0002-6777-4786; Email: ligy1999@gdut.edu.cn

Authors

Yunyun Zhang − *Guangdong-Hong Kong-Macao Joint Laboratory for Contaminants Exposure and Health, Guangdong Key Laboratory of Environmental Catalysis and Health Risk Control, Institute of Environmental Health and Pollution Control, Guangdong University of Technology, Guangzhou 510006, China; Guangzhou Key Laboratory of Environmental Catalysis and Pollution Control, Guangdong Basic Research Center of Excellence for Ecological Security and Green Development, School of Environmental Science and Engineering, Guangdong University of Technology, Guangzhou 510006, China*

Zhishu Liang − *Guangdong-Hong Kong-Macao Joint Laboratory for Contaminants Exposure and Health, Guangdong Key Laboratory of Environmental Catalysis and Health Risk Control, Institute of Environmental Health and Pollution Control, Guangdong University of Technology, Guangzhou 510006, China; Guangzhou Key Laboratory of Environmental Catalysis and Pollution Control, Guangdong Basic Research Center of Excellence for Ecological Security and Green Development, School of Environmental Science and Engineering, Guangdong University of Technology, Guangzhou 510006, China*

Po Keung Wong − *Guangdong-Hong Kong-Macao Joint Laboratory for Contaminants Exposure and Health, Guangdong Key Laboratory of Environmental Catalysis and Health Risk Control, Institute of Environmental Health and Pollution Control, Guangdong University of Technology, Guangzhou 510006, China; Guangzhou Key Laboratory of Environmental Catalysis and Pollution Control, Guangdong Basic Research Center of Excellence for Ecological Security and Green Development, School of Environmental Science and Engineering, Guangdong University of Technology, Guangzhou 510006, China;* orcid.org/0000-0003-3081-960X

Taicheng An − *Guangdong-Hong Kong-Macao Joint Laboratory for Contaminants Exposure and Health, Guangdong Key Laboratory of Environmental Catalysis and Health Risk Control, Institute of Environmental Health and*

https://doi.org/10.1021/acsestair.5c00326
ACS EST Air XXXX, XXX, XXX−XXX

Pollution Control, Guangdong University of Technology, Guangzhou 510006, China; Guangzhou Key Laboratory of Environmental Catalysis and Pollution Control, Guangdong Basic Research Center of Excellence for Ecological Security and Green Development, School of Environmental Science and Engineering, Guangdong University of Technology, Guangzhou 510006, China; orcid.org/0000-0001-6918-8070

Complete contact information is available at: https://pubs.acs.org/10.1021/acsestair.5c00326

Notes

The authors declare no competing financial interest.

■ ACKNOWLEDGMENTS

This work was supported by the National Key Research and Development Project (2023YFC3708204 and 2023YFC3708202) and the National Natural Science Foundation of China (42177410 and U25A20814).

■ REFERENCES

(1) Zuo, Y. Y.; Uspal, W. E.; Wei, T. Airborne transmission of COVID-19: Aerosol dispersion, lung deposition, and virus-receptor interactions. *ACS Nano* **2020**, *14* (12), 16502−16524.

(2) Li, C.; Tang, H. Comparison of COVID-19 infection risks through aerosol transmission in supermarkets and small shops. *Sustain. Cities Soc.* **2022**, *76*, 103424.

(3) Ma, J.; Shen, F.; Wang, M.; Sun, Y.; Li, C.; Teng, Y.; Mu, Q.; Chen, Y.; Zheng, Y.; Wu, Y.; Chen, S.; Zhu, T. Ecology of airborne microorganisms: Understanding the impact of haze and sandstorms on bacterial community structure and pathogenicity. *ACS EST Air* **2024**, *1* (11), 1402−1412.

(4) Damialis, A.; Gilles, S. Air quality in the era of climate change: Bioaerosols, multi-exposures, and the emerging threats of respiratory allergies and infectious diseases. *Curr Opin Environ Sci Health* **2025**, *46*, 100634.

(5) Wang, C. C.; Prather, K. A.; Sznitman, J.; Jimenez, J. L.; Lakdawala, S. S.; Tufekci, Z.; Marr, L. C. Airborne transmission of respiratory viruses. *Science* **2021**, *373* (6558), No. eabd9149.

(6) Guo, L.; Zhao, P. Y.; Jia, Y. K.; Wang, Z. F.; Chen, M.; Zhang, H.; Liu, D. X.; Zhang, Y.; Wang, X. H.; Rong, M. Z. Inactivation of airborne pathogenic microorganisms by plasma-activated nebulized mist. *J. Hazard. Mater.* **2023**, *459*, 132072.

(7) Kalisa, E.; Saini, A.; Lee, K.; Mastin, J.; Schuster, J. K.; Harner, T. Capturing the aerobiome: Application of polyurethane foam disk passive samplers for bioaerosol monitoring. *ACS EST Air* **2024**, *1* (5), 414−425.

(8) Iqbal, M. A.; Siddiqua, S. A.; Faruk, M. O.; Md Towfiqul Islam, A. R.; Salam, M. A. Systematic review and meta-analysis of the potential threats to respiratory health from microbial bioaerosol exposures. *Environ. Pollut.* **2024**, *341*, 122972.

(9) Qi, Y.; Chen, Y.; Yan, X.; Liu, W.; Ma, L.; Liu, Y.; Ma, Q.; Liu, S. Co-exposure of ambient particulate matter and airborne transmission pathogens: the impairment of the upper respiratory systems. *Environ. Sci. Technol.* **2022**, *56* (22), 15892−15901.

(10) Cornforth, D. M.; Diggle, F. L.; Melvin, J. A.; Bomberger, J. M.; Whiteley, M. Quantitative framework for model evaluation in microbiology research using *Pseudomonas aeruginosa* and cystic fibrosis infection as a test case. *Mbio* **2020**, *11* (1), No. e03042-19.

(11) Wang, Y. J.; Liu, Y.; Xue, S.; Chai, F. G.; Zhang, S.; Yang, K.; Liu, Y. F.; Li, J. L.; Yu, F. F. Comparative analysis of bioaerosol emissions: Seasonal dynamics and exposure risks in hospital vs. municipal wastewater treatment systems. *Environ. Pollut.* **2024**, *359*, 124608.

(12) Roy, R.; Jan, R.; Joshi, U.; Bhor, R.; Pai, K.; Satsangi, P. G. Characterization, pro-inflammatory response and cytotoxic profile of bioaerosols from urban and rural residential settings in Pune, India. *Environ. Pollut.* **2020**, *264*, 114698.

(13) Vincent, J. L.; Sakr, Y.; Singer, M.; Martin-Loeches, I.; Machado, F. R.; Marshall, J. C.; Finfer, S.; Pelosi, P.; Brazzi, L.; Aditianingsih, D.; Timsit, J. F.; Du, B.; Wittebole, X.; Maca, J.; Kannan, S.; Gorordo-Delsol, L. A.; De Waele, J. J.; Mehta, Y.; Bonten, M. J. M.; Khanna, A. K.; Kollef, M.; Human, M.; Angus, D. C. Prevalence and outcomes of infection among patients in intensive care units in 2017. *JAMA* **2020**, *323* (15), 1478−1487.

(14) Zhang, D.; Bond, T.; Pan, Y.; Li, M. L.; Luo, J. Y.; Xiao, R.; Chu, W. H. Identification, occurrence, and cytotoxicity of haloanilines: a new class of aromatic nitrogenous disinfection byproducts in chloraminated and chlorinated drinking water. *Environ. Sci. Technol.* **2022**, *56* (7), 4132−4141.

(15) Shen, F. L.; Li, D.; Guo, J. H.; Chen, J. M. Mechanistic toxicity assessment of differently sized and charged polystyrene nanoparticles based on human placental cells. *Water Res.* **2022**, *223*, 118960.

(16) Wang, Y. J.; Zhang, S.; Yang, L. Y.; Yang, K.; Liu, Y.; Zhu, H. R.; Lai, B. S.; Li, L.; Hua, L. L. Spatiotemporal distribution, interactions and toxic effect of microorganisms and ARGs/MGEs from the bioreaction tank in hospital sewage treatment facility. *Sci. Total Environ.* **2024**, *923*, 171481.

(17) Bessa, M. J.; Brandao, F.; Rosário, F.; Moreira, L.; Reis, A. T.; Valdiglesias, V.; Laffon, B.; Fraga, S.; Teixeira, J. P. Assessing the *in vitro* toxicity of airborne (nano)particles to the human respiratory system: from basic to advanced models. *J. Toxicol. Environ. Health, Part B* **2023**, *26* (2), 67−96.

(18) Malet, J. K.; Hennemann, L. C.; Hua, E. M. L.; Faure, E.; Waters, V.; Rousseau, S.; Nguyen, D. A model of intracellular persistence of *Pseudomonas aeruginosa* in airway epithelial cells. *Cell. Microbiol.* **2022**, *2022*, 5431666.

(19) Fernandez, M. O.; Thomas, R. J.; Oswin, H.; Haddrell, A. E.; Reid, J. P. Transformative approach to investigate the microphysical factors influencing airborne transmission of pathogens. *Appl. Environ. Microbiol.* **2020**, *86* (23), No. e01543-20.

(20) Rothen-Rutishauser, B.; Gibb, M.; He, R. W.; Petri-Fink, A.; Sayes, C. M. Human lung cell models to study aerosol delivery-considerations for model design and development. *Eur. J. Pharm. Sci.* **2023**, *180*, 106337.

(21) Rijsbergen, L. C.; van Dijk, L. L. A.; Engel, M. F. M.; de Vries, R. D.; de Swart, R. L. In vitro modelling of respiratory virus infections in human airway epithelial cells a systematic review. *Front. Immunol.* **2021**, *12*, 683002.

(22) Lakhdar, R.; Mumby, S.; Abubakar-Waziri, H.; Porter, A.; Adcock, I. M.; Chung, K. F. Lung toxicity of particulates and gaseous pollutants using *ex-vivo* airway epithelial cell culture systems. *Environ. Pollut.* **2022**, *305*, 119323.

(23) Nogueira, L. S.; Vasconcelos, C. P.; Mitre, G. P.; Bittencourt, L. O.; Plaça, J. R.; Kataoka, M. S. D.; Pinheiro, J. D. V.; Garlet, G. P.; De Oliveira, E. H. C.; Lima, R. R. Gene expression profile in immortalized human periodontal ligament fibroblasts through hTERT ectopic expression: transcriptome and bioinformatic analysis. *Front. Mol. Biosci.* **2021**, *8*, 679548.

(24) Wang, H. Y.; Peng, L. H.; Li, G. Y.; Liu, H. L.; Liang, Z. S.; Zhao, H. J.; An, T. C. Enhanced catalytic ozonation inactivation of bioaerosols by MnO_2/Ni foam with abundant vacancies and at concentration. *Appl. Catal. B Environ. Energy* **2024**, *344*, 123675.

(25) Yang, Y. M.; Yang, L.; Hu, X. Y.; Shen, Z. X. Characteristics of bioaerosols under high-ozone periods, haze episodes, dust storms, and normal days in Xi'an, China. *Particuology* **2024**, *90*, 140−148.

(26) Chen, T. T.; Cai, Y. W.; Sun, T.; Liao, W.; Li, G. Y.; Liang, Z. S.; An, T. C. Response and formation mechanism of highly antibiotic-resistant dormant subpopulations in bioaerosol during aerosolizing from aquatic environments. *Environ. Sci. Technol.* **2025**, *59* (41), 22145−22156.

(27) Li, Z. H.; Xu, T.; Li, X. J.; Wang, T. J.; Tang, G. B.; Zhao, H. H.; Zhao, Y. L.; Ye, K.; Gao, P. Viral integration promotes SV40T-induced immortalization by disturbing the expression of DNA/

chromosome- and ECM-associated functional genes. *Gene* **2024**, *896*, 148060.
(28) Wu, X.; Zhou, L. T.; Ye, C.; Zha, Z. Z.; Li, C. C.; Feng, C.; Zhang, Y.; Jin, Q.; Pan, J. Y. Destruction of self-derived PAMP via T3SS2 effector VopY to subvert PAMP-triggered immunity mediates *Vibrio parahaemolyticus* pathogenicity. *Cell Rep.* **2023**, *42* (10), 113261.
(29) Wood, S. J.; Goldufsky, J. W.; Seu, M. Y.; Dorafshar, A. H.; Shafikhani, S. H. *Pseudomonas aeruginosa* cytotoxins: Mechanisms of cytotoxicity and impact on inflammatory responses. *Cells* **2023**, *12* (1), 195.
(30) Jain, A.; Mittal, S.; Tripathi, L. P.; Nussinov, R.; Ahmad, S. Host-pathogen protein-nucleic acid interactions: A comprehensive review. *Comput. Struct. Biotechnol. J.* **2022**, *20*, 4415−4436.
(31) Häder, A.; Schäuble, S.; Gehlen, J.; Thielemann, N.; Buerfent, B. C.; Schüller, V.; Hess, T.; Wolf, T.; Schröder, J.; Weber, M.; Hünniger, K.; Löffler, J.; Vylkova, S.; Panagiotou, G.; Schumacher, J.; Kurzai, O. Pathogen-specific innate immune response patterns are distinctly affected by genetic diversity. *Nat. Commun.* **2023**, *14* (1), 3239.
(32) Zhang, T. W.; Zhong, Y.; Shi, Y.; Feng, C. C.; Xu, L.; Chen, Z.; Sun, X.; Zhao, Y.; Sun, X. L. Multi-omics reveals that 5-O-methylvisammioside prevention acute liver injury in mice by regulating the TNF/MAPK/NF-κB/arachidonic acid pathway. *Phytomedicine* **2024**, *128*, 155550.
(33) Chen, B. D.; Mu, C. L.; Zhang, Z. W.; He, X. L.; Liu, X. The love-hate relationship between TGF-*β* signaling and the immune system during development and tumorigenesis. *Front. Immunol.* **2022**, *13*, 891268.
(34) Mogensen, T. H. Pathogen recognition and inflammatory signaling in innate immune defenses. *Clin. Microbiol. Rev.* **2009**, *22* (2), 240−273.
(35) Chen, J. X.; Qi, D. J.; Hu, H. R.; Wang, X. J.; Lin, W. L. Unconventional posttranslational modification in innate immunity. *Cell. Mol. Life Sci.* **2024**, *81* (1), 290.
(36) Loaiza-Moss, J.; Braun, U.; Leitges, M. Transcriptome profiling of mouse embryonic fibroblast spontaneous immortalization: a comparative analysis. *Int. J. Mol. Sci.* **2024**, *25* (15), 8116.
(37) Philips, R. L.; Wang, Y.; Cheon, H.; Kanno, Y.; Gadina, M.; Sartorelli, V.; Horvath, C. M.; Darnell, J. E.; Stark, G. R.; O'Shea, J. J. The JAK-STAT pathway at 30:Much learned, much more to do. *Cell* **2022**, *185* (21), 3857−3876.

https://doi.org/10.1021/acsestair.5c00326
ACS EST Air XXXX, XXX, XXX−XXX